Bulletin of the Seismological Society of America, Vol. 94, No. 5, pp. 1630–1643, October 2004

Frequency-Dependent *Lg Q* within the Continental United States

by Dirk Erickson, Daniel E. McNamara, and Harley M. Benz

Abstract Frequency-dependent crustal attenuation ($1/Q$) is determined for seven distinct physiographic/tectonic regions of the continental United States using high-quality *Lg* waveforms recorded on broadband stations in the frequency band 0.5 to 16 Hz. *Lg* attenuation is determined from time-domain amplitude measurements in one-octave frequency bands centered on the frequencies 0.75, 1.0, 3.0, 6.0, and 12.0 Hz. Modeling errors are determined using a delete-j jackknife resampling technique. The frequency-dependent quality factor is modeled in the form of $Q = Q_0 f^{\eta}$. Regions were initially selected based on tectonic provinces but were eventually limited and adjusted to maximize ray path coverage in each area. Earthquake data was recorded on several different networks and constrained to events occurring within the crust (<40 km depth) and at least m_b 3.5 in size. A singular value decomposition inversion technique was applied to the data to simultaneously solve for source and receiver terms along with Q for each region at specific frequencies. The lowest crustal Q was observed in northern and southern California where Q is described by the functions $Q = 152(\pm 37)f^{0.72(\pm 0.16)}$ and $Q = 105(\pm 26)f^{0.67(\pm 0.16)}$, respectively. The Basin and Range Province, Pacific Northwest, and Rocky Mountain states also display lower Q and a strong frequency dependence characterized by the functions $Q = 200(\pm 40)f^{0.68(\pm 0.12)}$, $Q = 152(\pm 49)f^{0.76(\pm 0.18)}$, and $Q = 166(\pm 37)f^{0.61(\pm 0.14)}$, respectively. In contrast, in the central and northeast United States Q functions are $Q = 640(\pm 225)f^{0.344(\pm 0.22)}$ and $Q = 650(\pm 143)f^{0.36(\pm 0.14)}$, respectively, show a high crustal Q and a weaker frequency dependence. These results improve upon previous *Lg* modeling by subdividing the United States into smaller, distinct tectonic regions and using significantly more data that provide improved constraints on frequency-dependent attenuation and errors. A detailed attenuation map of the continental United States can provide significant input into hazard map mitigation. Both scattering and intrinsic attenuation mechanisms are likely to play a comparable role in the frequency range considered in the study.

Introduction

Regional attenuation calculations have been derived from the arrival and measurement of *Lg* wave amplitudes recorded at broadband stations across the continental United States. A large amount of new earthquake data allows us to create a detailed attenuation map of the United States, which will provide the hazard community with valuable information about shaking intensities at various frequencies for the design of structures including bridges, buildings, and dams. Variations in the attenuation of seismic waves in different tectonic regions were noticed prior to modern day instrumentation when the shaking intensity of earthquakes in the western United States diminished faster with epicentral distance than that of earthquakes of comparable size in the central and eastern United States (Nuttli *et al.*, 1979; Singh and Herrmann, 1983). Recent studies utilizing modern digital seismic instruments have confirmed that attenuation is noticeably higher, as much as six times, in the western United States (Mitchell, 1975; Frankel *et al.*, 1990; Benz *et al.*, 1997).

The acceptance of lateral heterogeneities within the crust has been widely acknowledged since the latter half of the previous century (Smithson, 1978; Christensen and Mooney, 1995). Therefore, *Lg* propagation is influenced by disparities in the crustal wave guide along its travel path. High attenuation has been suggested to be caused by several mechanisms, including highly fractured crust in tectonically active regions that effectively absorb high-frequency seismic waves (Aki, 1980), elevated crustal temperatures (Frankel, 1991), and variations in crustal thickness and structures that control elastic-wave propagation (Gregersen, 1984).

Lg appears as the dominant high-frequency phase in regional seismic waveforms and is used extensively to deter-

mine a variety of effects that include earthquake source parameters, site response, *S*-wave velocity, and attenuation (Atkinson and Mereu, 1992). *Lg* is generated by a superposition of higher-mode surface waves (Oliver and Ewing, 1957; Mitchell, 1975) or multiple reflected shear energy within the crustal waveguide (Gutenberg, 1955), which travels with a group velocity of about 3.5 km/sec. Since *Lg* loses energy quickly within transition zones where crustal thicknesses change drastically from either large to small or small to large, constant crustal thicknesses are needed to provide an effective waveguide (Kennett, 1986). In stable tectonic regions, such as North Africa, *Lg* has been observed at distances as great as 6000 km (McNamara and Walter, 2001), but in areas comparable to northern California, *Lg* can be completely attenuated by local geology in less than 500 km.

Although there have been numerous studies to determine frequency-dependent *Lg* attenuation for the continental United States (Nuttli, 1973; Mitchell, 1975; Frankel, 1991; Benz *et al.*, 1997), this is the first study to define *Lg Q* for three new regions and to incorporate a relatively large data set to produce a detailed *Q* map of the continental United States. In this article, we study the nature of *Lg* propagation and attenuation within seven regions of the continental United States. To accomplish this, seismic waveforms were first visually inspected for the presence of *Lg* amplitudes, and then *Lg* amplitudes were inverted for paths restricted to specific, predetermined tectonic regions. The frequency-dependent quality factor *Q* is commonly modeled using the power law in the form

$$Q(f) = Q_0(f/f_0)^{\eta},$$

where f_0 is a reference frequency ($f_0 = 1$ for this work), Q_0 is Q at the reference frequency, and η is assumed to be constant over the frequencies of interest.

Data Selection

The *Lg* waveform data used in this study were acquired from January 2000 to February 2003 from local and regional earthquakes recorded by three-component broadband stations of the U.S. National Seismic Network, Global Seismic Network (GSN), Regional Seismic Network, and other cooperative stations, which comprise the backbone of the Advanced National Seismic System (Table 1). Consistent processing and interpretation of the *Lg* attenuation results was made possible by the availability of high-quality, calibrated waveforms from various regions of the United States, Canada, and Mexico which were fed in real time to the U.S. Geological Survey at the National Earthquake Information Center. The event locations were determined from the USGS's Preliminary Determination of Epicenters catalog.

For our analysis, seven different regions across the continental United States were selected based on tectonic boundaries and ray path coverage. To reduce the trade-off between source and receiver terms in the inversion, only station–event pairs were used that had a minimum of three observations. The three new regions that have not been previously studied for *Lg Q* include northern California, the Pacific Northwest, and the mountain states, while the previously studied regions are southern California, the Basin and Range Province, the central United States, and the northeast United States.

Amplitude measurement of the *Lg* waveform is similar to the method utilized by McNamara *et al.* (2000) and Benz *et al.* (1997). Waveforms are visually inspected for the presence of *Lg* on the vertical component at the appropriate time for a wave traveling at a typical continental *Lg* velocity (3.0 to 3.6 km/sec) (McNamara *et al.*, 1996). A qualitative analysis based on signal-to-noise ratio (SNR) was then used to select *Lg* waveforms for the inversion. Instruments were deconvolved from velocity seismograms, resulting in absolute ground displacement in meters. For each path, *Lg* amplitudes were measured in the frequency domain using a root mean squares (rms) technique on whole octaves for five passbands with center frequencies at 0.75, 1.5, 3.0, 6.0, and 12.0 Hz. For example, we measured an rms over 2.0 to 4.0 Hz for the center frequency of 3.0 Hz to reduce the variance of amplitudes over whole octaves instead of measuring peak amplitudes, which could be influenced by outliers. *Lg* was observed within a range of path lengths from several tens of kilometers to several thousand kilometers. Path lengths were limited to those greater than 110 km because short epicentral distances made it difficult to determine the presence of *Lg* due to the interference of the local, faster *S* arrivals. Greater epicentral distances allowed the faster *S* waves to separate from the slower *Lg* waves, making it easier to distinguish between the two arrivals. Earthquake data was limited to those events greater than m_b 3.5, and earthquake depths were restricted to less than 40 km to ensure that the *Lg* waves were generated and remained in the crust.

Methods

The inversion technique used in this study to estimate the frequency dependence of *Lg* is described in detail by Benz *et al.* (1997) and McNamara *et al.* (1996).

The observed amplitude of *Lg* can be modeled as

$$A(f,D) = (1/D^{\gamma})\, R(f)S(f)\mathrm{e}^{-\pi fD/vQ(f)}, \qquad (1)$$

where D is the hypocentral distance, γ is the exponent of the geometric spreading within the medium, R is the receiver term that denotes site effects, S is the term that represents the individual earthquake source excitation, f is the median frequency of the observed wave, v is the group velocity for *Lg* (3.5 km/sec), and $Q(f)$ is the quality factor of *Lg* propagation within the crust.

Rewriting and taking the natural log of both sides to linearize the above equation yields

Table 1
Seismic Stations, Locations, Number of Recorded Earthquakes, and Region in This Study

Station	Latitude	Longitude	No. Observations	Region
AHID	42.7654	−111.1004	44	Mtn. States
BEKR	39.8667	−120.3586	40	N. California
BINY	42.199	−75.986	28	NE USA
BLO	39.172	−86.522	12	Central USA
BMN	40.4314	−117.2217	39	Basin & Range/Pacific NW
BOZ	45.5999	−111.1633	46	Mtn. States
BRYW	41.918	−71.539	1	NE USA
BW06	42.7777	−109.5555	53	Mtn. States
CBKS	38.814	−99.7373	33	Central USA
CBN	38.205	−77.373	6	NE USA
CCM	38.0556	−91.2445	27	Central USA
CMB	38.035	−120.385	57	N. California
COR	44.5857	−123.3031	11	Pacific NW
CTU	40.6925	−111.7503	28	Basin & Range
DAC	36.277	−117.5937	33	S. California/Basin & Range
DUG	40.195	−112.8133	65	Basin & Range
ELK	40.7448	−115.2387	56	Basin & Range/Pacific NW
GNAR	35.965	−90.018	4	Central USA
GOGA	33.411	−83.467	18	Central USA
GWDE	38.826	−75.617	7	NE USA
HAWA	46.3925	−119.5323	37	Pacific NW
HLID	43.563	−114.414	71	Pacific NW/Mtn. States
HNH	43.705	−72.286	10	NE USA
HOPS	38.994	−123.072	18	N. California
HRV	42.506	−71.558	12	NE USA
HVU	41.78	−112.775	53	Basin & Range/Mtn. States
HWUT	41.6073	−111.565	71	Basin & Range/Mtn. States
ISA	35.6633	−118.4733	52	S. California
KNB	37.0166	−112.8224	26	Basin & Range
LBNH	44.24	−71.926	24	NE USA
LKWY	44.5651	−110.4	33	Mtn. States
LRAL	33.035	−86.998	11	Central USA
LSCT	41.678	−73.224	20	NE USA
MCWV	39.6581	−79.8456	17	NE USA
MIAR	34.5457	−93.573	31	Central USA
MNV	38.4328	−118.1531	58	Basin & Range
MOD	41.9033	−120.3058	40	N. California/Pacific NW
MPU	40.016	−111.63	20	Basin & Range
MSO	46.8292	−113.9406	24	Pacific NW/Mtn. States
MVU	38.504	−112.21	32	Basin & Range
MYNC	35.074	−84.128	9	Central USA
NCB	43.971	−74.224	24	NE USA
NEW	48.2633	−117.12	42	Pacific NW
NOQ	40.653	−112.12	10	Basin & Range
OCWA	47.749	−124.178	10	Pacific NW
OXF	34.512	−89.409	28	Central USA
PAHR	39.7065	−119.3841	15	Basin & Range/N. California
PAL	41.006	−73.908	22	Central USA/NE USA
PAS	34.148	−118.17	6	S. California
PFO	33.6091	−116.4552	32	S. California
PGC	48.65	−123.45	3	Pacific NW
SAO	36.765	−121.445	39	S. California
SIUC	37.715	−89.218	18	Central USA
SLM	38.636	−90.236	6	Central USA
SNCC	33.248	−119.524	2	S. California
SPW	47.554	−122.25	1	Pacific NW
SSPA	40.636	−77.888	23	NE USA
SWET	35.216	−85.932	3	Central USA
TPH	38.075	−117.2225	53	Basin & Range
TPNV	36.9286	−116.2236	77	S. California/Basin & Range
UALR	34.775	−92.344	7	Central USA

(*continued*)

Table 1
Continued

Station	Latitude	Longitude	No. Observations	Region
VTV	34.567	−117.33	1	S. California
WALA	49.058	−113.92	20	Pacific NW/Mtn. States
WCI	38.229	−86.294	23	Central USA
WCN	39.3106	−119.7563	34	Basin & Range/N. California
WDC	40.58	−122.5397	29	N. California/Pacific NW
WES	42.385	−71.322	3	NE USA
WMOK	34.738	−98.781	36	Central USA
WVL	44.565	−69.658	5	NE USA
WVOR	42.4339	−118.6367	34	Basin & Range/Pacific NW
WVT	36.13	−87.83	27	Central USA
YBH	41.7318	−122.7105	20	N. California/Pacific NW
YMR	44.669	−110.97	22	Mtn. States

$$\ln A(f) + \gamma \ln D = \ln R(f) + \ln S(f) - \pi f D/vQ(f). \quad (2)$$

When the left-hand side of this equation is plotted against epicentral distance, the right-hand side describes a line where the R and S terms control the intercept and the Q term controls the slope.

Since the responses of most of our instruments are well known, it is possible to directly solve for the source and receiver terms along with the regional Q value by inverting instrument-corrected and geometrical spreading–corrected *Lg* amplitudes from many different events (Benz *et al.*, 1997). With such a large data set of source-receiver pairs, it is possible to set up a system of linear equations based on equation (2). The system of equations can be expressed as

$$\mathbf{Ax} = \mathbf{t}, \quad (3)$$

where **A** is the system matrix made up of the parameter coefficients of equation (2), **x** is a column vector containing the unknown event (S) and station (R) terms and the regional Q term, and the **t** vector comprises the left-hand side of equation (2). The system matrix, **A**, is made up of mostly ones and zeros, with the last column listing $-(\pi fD/v)$, a portion of the last term of equation (2). By solving for each frequency independently, the known variables are f, D, and v for each source–receiver pair. A singular value decomposition (SVD) inversion technique is then applied to determine the unknown variables, S, R, and Q, for each frequency in every region. As a test, a least-squares inversion was also applied to the data, which produced identical results to the SVD inversion.

The inversions were performed for five different whole-octave frequency bands with center frequencies at 0.75, 1.5, 3.0, 6.0, and 12.0 Hz for each of the regions to obtain a unique measure of frequency-dependent $Q(f)$. Since the effects of scattering or radiation pattern cannot be separated in this work, and a reasonable, constant geometric spreading rate is assumed, our results represent an apparent Q. Since *Lg* is a multiply reflected scattered wave that distributes energy across all three components of motion, radiation effects should be minimal (McNamara *et al.*, 1996).

We made several assumptions in the *Lg* $Q(f)$ computation. Based on the qualitative analysis of the data from the continental United States, we observed that the main *Lg* energy arrived within the group velocity window 3.6 to 3.1 km/sec. A frequency-independent group velocity of 3.5 km/sec was assumed based on this observation and the fact that *Lg* is not dispersive (Gutenberg, 1955).

An arbitrary reference station was selected to normalize the remaining stations. The reference station was chosen based on low background noise and well-known response characteristics, but in the end, the choice of reference station had no effect on Q. Selection of a reference station is critical when determining relative receiver terms, but this topic is not discussed in this article.

Since it is difficult to simultaneously solve for the geometric spreading and attenuation, the geometric spreading term γ is assumed to remain constant at 0.5 for each region and frequency (Benz *et al.*, 1997).

Error Analysis

We examined the mean and standard deviation of Q for each region for all frequencies by resampling the original dataset using the delete-j jackknife resampling technique modeled after the method of Efron and Tibshirani (1993). To achieve consistency for the jackknife estimate of standard deviation, we left out at least $d = \sqrt{n}$, where n is the total number of observations and d is the number of observations removed from the complete dataset (Efron and Tibshirani, 1993). To obtain an error bound, we removed (d) number of randomly selected observations from the total (n) number of observations to create 1000 new jackknife datasets, and then inverted each jackknife dataset to determine 1000 Q values. From these 1000 Q values, we were able to calculate a standard deviation and mean value for the region at a desired frequency. We used 2σ for our error bound and compared the mean Q to the actual Q computed from the entire dataset to test for stability and accuracy.

Figure 1 shows a histogram of the results obtained from 2000 different inversions of randomly selected jackknife datasets from the northern California region at 1.5 Hz. We used 2000 inversions for this example instead of the standard 1000 inversions to show that standard deviations do not change for more jackknife datasets and the distribution trends toward normal. We removed 10 different randomly selected observations from the complete dataset ($n = 85$) to create 2000 new jackknife datasets, and then inverted each jackknife dataset to obtain 2000 Q values.

The mean and standard deviation were calculated from this set of 2000 Q values to establish error estimates for the region. In this example, the complete dataset Q is 127 and the standard deviation is 2.6, therefore $Q = 127 (\pm 5)$ at 1.5 Hz. The distribution appears to be normal with a noticeable peak at about 127, which corresponds to both the Q calculated from the entire dataset and the mean jackknife value of Q.

We also tested the stability of our datasets by removing an increasing number of observations to determine where the dataset becomes unstable. The same dataset used previously remained stable, with a standard deviation less than 30 and a delta Q less than 5, until about 70% of the data was removed (Fig. 2). This suggests that Q can be determined with relatively few observations, and that adding more observations merely decreases the error. This also reinforces our selection of tectonic regions in that Q is a reasonable estimate of the region average.

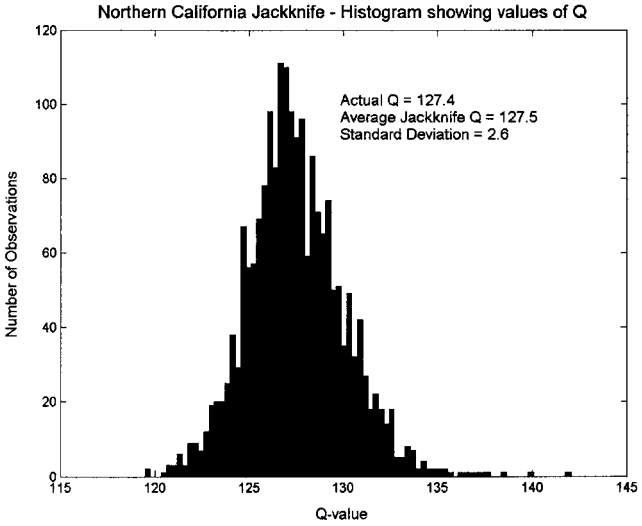

Figure 1. Histogram of 2000 jackknife Q inversions for northern California region at 1.5 Hz. In this example, total number of observations (n) = 85 and number of observations removed for each jackknife inversion (d) = 10. Note normal distribution of Q values. Actual Q value is 127.4. Average jackknife Q value is 127.5, with a difference of only 0.1.

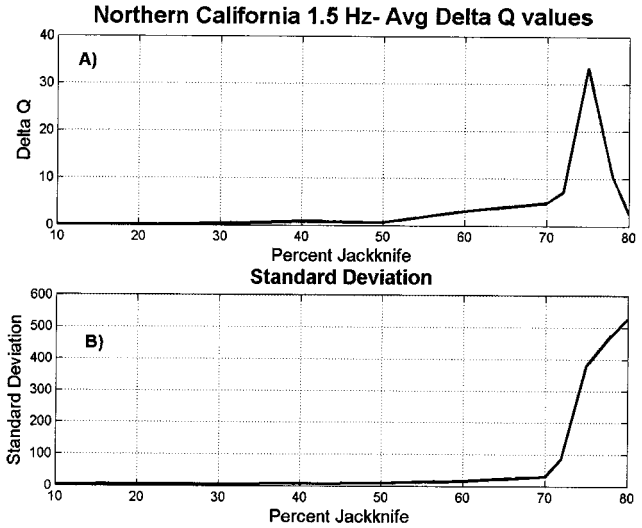

Figure 2. Plot A shows the difference between the average jackknife Q and the actual Q value versus the percent of data removed from the original dataset before inverting for Q. Note that the dataset is relatively stable until about 70% of the data is removed. Plot B shows the standard deviation versus percent of data removed from the original dataset before inversion. Note that the standard deviation also remains low and stable until about 70% of the original data is removed.

Results

From the inversion results, we observe that tectonically stable regions such as the central United States generally have the highest Q_0 values and the weakest frequency dependence (low η), while tectonically active regions generally have low Q_0 values and high η values.

Southern California

Figure 3A shows the distribution of broadband stations (triangles), earthquakes (circles), and source–receiver *Lg* paths (solid lines) for the southern California region at 3 Hz. The maps were constructed at 3 Hz because this frequency represents the portion of the frequency band of interest with the best SNR, thus providing a view of ray-path coverage in each area. This region, ranging from 30°N to 37°N and 114°W to 122°W, includes the southern Coast Ranges, southern Sierra Nevada, and a portion of the eastern Mojave and extensional region east of the Sierra Nevada and is covered by 58 ray paths induced by 17 earthquakes and recorded at 5 stations. The focus here is to characterize the San Andreas fault system. Several earthquakes and stations, such as the station on San Nicolas Island, were not used in this example because of noisy data or comparatively few spectral measurements.

Figure 3B shows a comparison of *Lg* spectral amplitude versus epicentral distance at center frequencies of 0.75, 1.5, 3.0, 6.0, and 12 Hz, corrected for source and receiver terms determined from the inversion. An L2 norm best-fit line was also applied to the corrected *Lg* amplitudes to show a linear trend in the data. The reference station for southern California is TPNV, which is located in southwestern Nevada. The

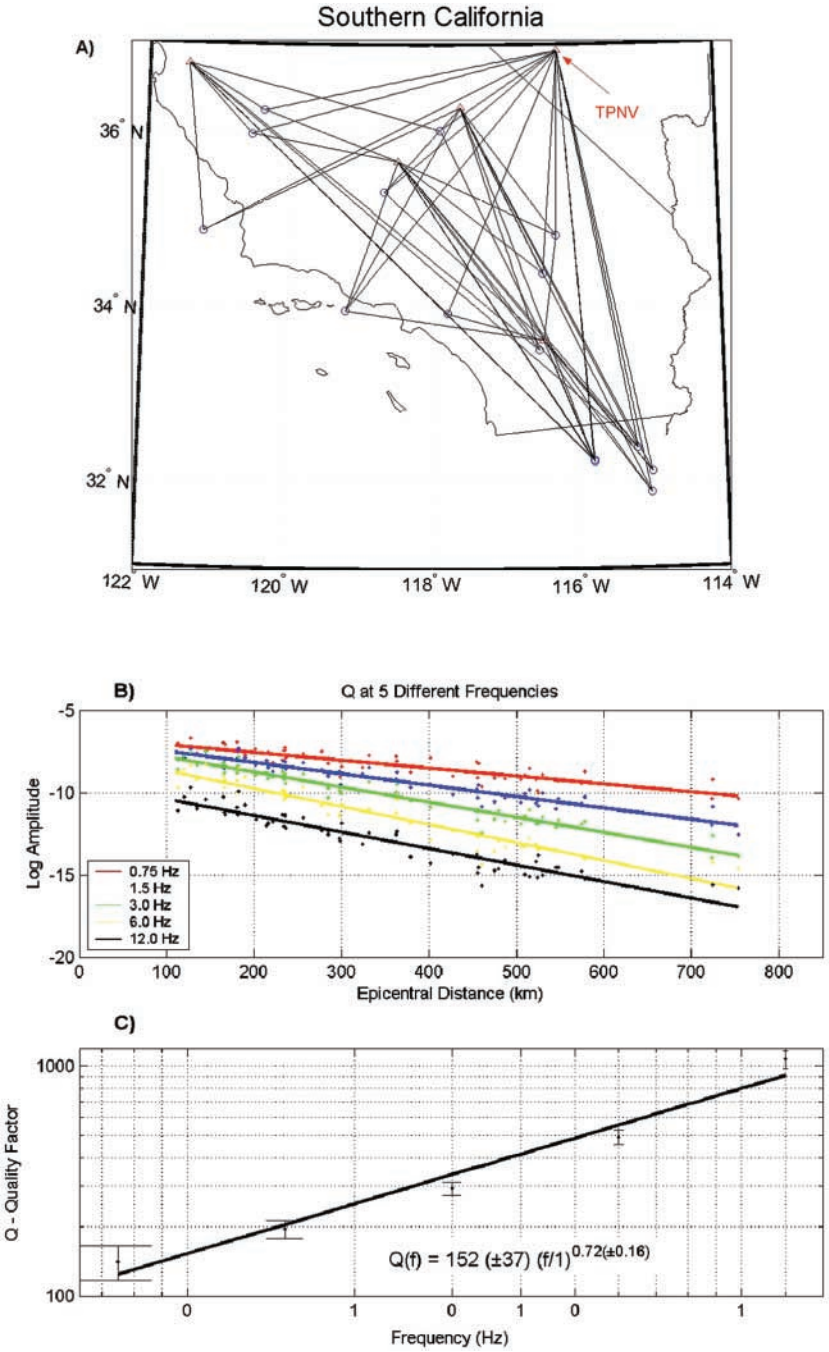

Figure 3. A, Map of southern California study area sampled at 3 Hz. Triangles are broadband stations, circles are events, and lines represent station–receiver *Lg* ray paths used in this region. This area is covered by 58 ray paths from 17 earthquakes recorded at 5 stations. Region ranges from 30°N to 37°N and 114°W to 122°W. B, Southern California *Lg* spectral amplitudes (dots) at 0.75, 1.5, 3.0, 6.0, and 12.0 Hz, corrected for source and receiver terms. Solid line is a best-fit linear trend for data assuming frequency-independent Q and $\gamma = 0.5$. Plus and minus terms for Q are derived from the standard deviation of the jackknife method described above and equate to 2σ. C shows the five values of *Lg* for each center frequency with corresponding error bars plotted on a log–log graph to exhibit the linear frequency dependence of the southern California region. The best-fit frequency-dependent *Lg* Q function is $Q(f) = 152\ (\pm 37)\ (f/1)^{0.72(\pm 0.16)}$, where the plus and minus terms are the error terms for the best-fit line.

results show an increase in *Lg* Q from 141 (± 24) at 0.75 Hz to 1074 (± 92) at 12.0 Hz. The error terms, denoted by the plus and minus values, are 2σ standard deviations computed from the jackknife method described above. Generally, the standard deviation is relatively small at the middle frequencies (1.5, 3.0, and 6.0 Hz) and increases at the two end frequencies (0.75 and 12.0 Hz). This may be due to the fact that there are fewer ray paths at 12.0 Hz due to variation in instrumentation, and because of stronger effects of radiation pattern at lower frequencies that are not corrected for in the inversion (Benz *et al.*, 1997). GSN stations record at 20 samples per second (Nyquist frequency = 10 Hz), so it is impossible to sample true energy levels in the octave band 8–16 Hz with a center frequency of 12 Hz.

By plotting the Q values and error terms for each of the five frequencies on a log–log scale, we see a frequency-dependent $Q(f)$ function emerge (Fig. 3C). We then fit a linear trend to the data using an L2 norm to produce a best-fit frequency-dependent *Lg* Q function of $Q(f) = 152\ (\pm 37)\ (f/1)^{0.72(\pm 0.16)}$ for the region. Our results vary slightly from those of Benz *et al.* (1997) who used similar inversion techniques but fewer source–receiver raypaths to resolve a frequency-dependent *Lg* Q function of $Q(f) = 187\ (\pm 7)\ (f/1)^{0.55(\pm 0.03)}$ between 1.0 and 7.0 Hz. Our results are also

consistent with the crustal coda Q results of Singh and Herrmann (1983) who find an average Q_0 of 200 and η of 0.6 for southern California.

Basin and Range

The Basin and Range Province is characterized by high heat flow and thin continental crust in a tectonically active environment. This region is mainly made up of Nevada and western Utah but has several stations or events in southern Oregon, California, and Idaho. Figure 4A shows a map of the Basin and Range Province defined by the coordinates 36°N to 42.5°N and from 111°W to 120°W, with corresponding ray paths, stations, and earthquakes used in this study.

The Basin and Range Province is well sampled, with 242 ray paths from 31 sources recorded by 17 stations. The best-fit lines to the *Lg* spectral amplitudes, corrected for source and receiver terms, are shown in Figure 4B. Station DUG, located in west-central Utah, is used as the reference station. Results show that *Lg Q* increases from 183 (±8) at 0.75 Hz to 1255 (±54) at 12.0 Hz (Fig. 4B).

Like southern California, the Basin and Range Province shows a strong frequency-dependent *Lg Q* with an equation of $Q(f) = 200\ (\pm 77)\ (f/1)^{0.69(\pm 0.16)}$ (Fig. 4C). Chavez and Priestley (1986) also found similar results with a frequency-dependent *Lg Q* function of $Q(f) = 206\ f^{0.68}$ between the frequencies of 0.3 and 10.0 Hz with approximately 40 ray

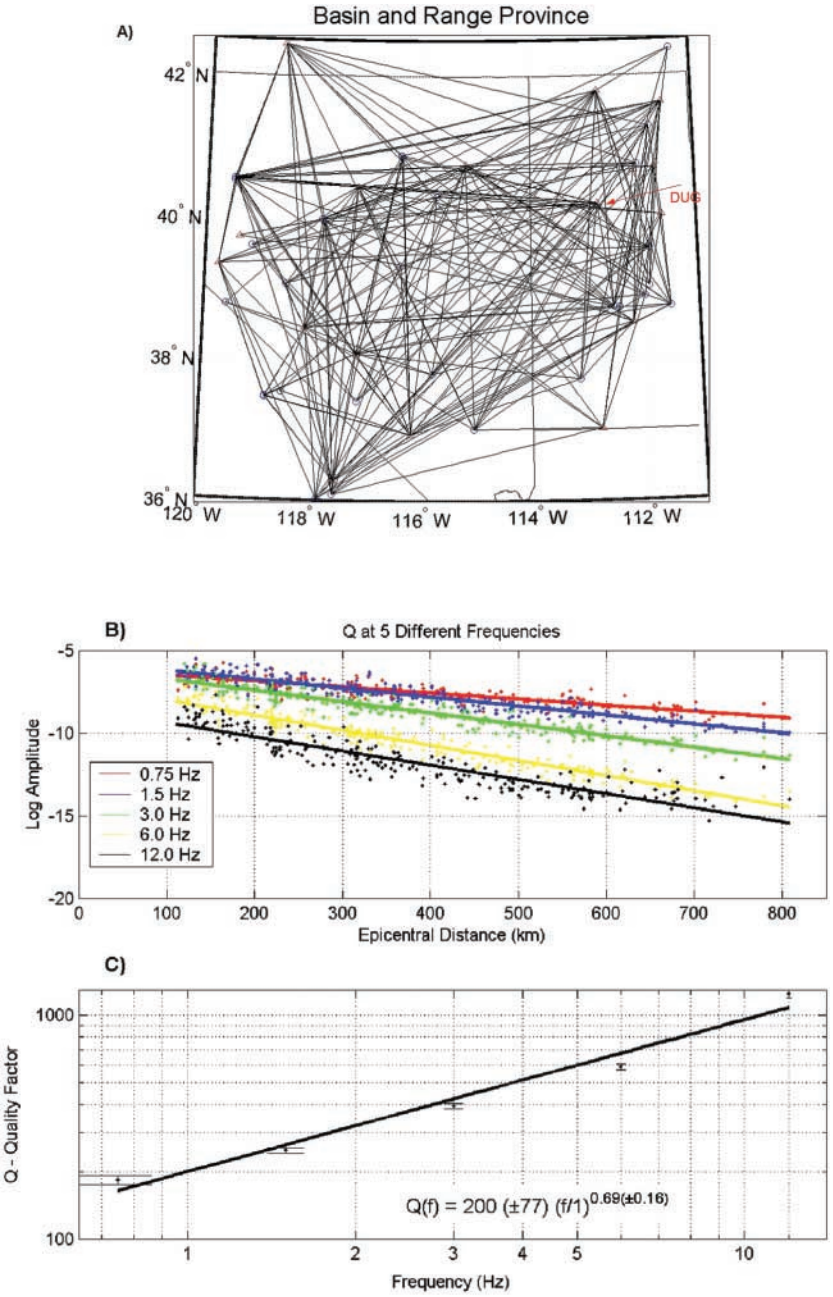

Figure 4. A, Basin and Range Province sampled at 3 Hz. Triangles are broadband stations, circles are events, and lines represent *Lg* source–receiver ray paths used in this study. This area is covered by 242 ray paths, 31 earthquakes, and 17 stations. The coordinates for this province are 36°N to 42.5°N and 111°W to 120°W. B, Basin and Range Province *Lg* spectral amplitudes (dots) at 0.75, 1.5, 3.0, 6.0, and 12.0 Hz, corrected for source and receiver terms. Solid line is best-fit linear trend for data assuming frequency-independent Q and $\gamma = 0.5$. C contains the five values for Q at each center frequency with corresponding error bars and a best-fit linear trend plotted on a log–log graph to show a frequency-dependent Q. The best-fit frequency-dependent *Lg Q* function is $Q(f) = 200\ (\pm 77)\ (f/1)^{0.69(\pm 0.16)}$ between 0.75 and 12.0 Hz.

paths. Our Q function is also close to that determined by Benz *et al.* (1997) for their results between 1.0 and 5.0 Hz with $Q(f) = 235\ (\pm 11)\ (f/1)^{0.56(\pm 0.04)}$ for 90 ray paths. Coda Q values presented by Xie and Mitchell (1990) are slightly different, with a Q_c value of 267 (± 56) and a somewhat less frequency-dependent η value of 0.37 (± 0.06). The east African rift is tectonically similar to the Basin and Range Province, exhibiting active continental tectonics and a thin crust with a frequency-dependent *Lg* Q of $Q(f) = 186\ (\pm 7)\ f^{0.78(\pm 0.05)}$ (Ferdinand, 1998).

Northern California

The northern California region is defined by 85 ray paths from 18 earthquakes recorded at seven stations, with coordinates of 37°N to 42°N and 119°W to 125°W (Fig. 5A). This classic subduction zone region has no prior *Lg* Q results. Current attenuation numbers are necessary for hazard map mitigation in this densely populated area that has been subjected to large earthquakes. The best-fit lines to the *Lg* spectral amplitudes, corrected for source and receiver terms,

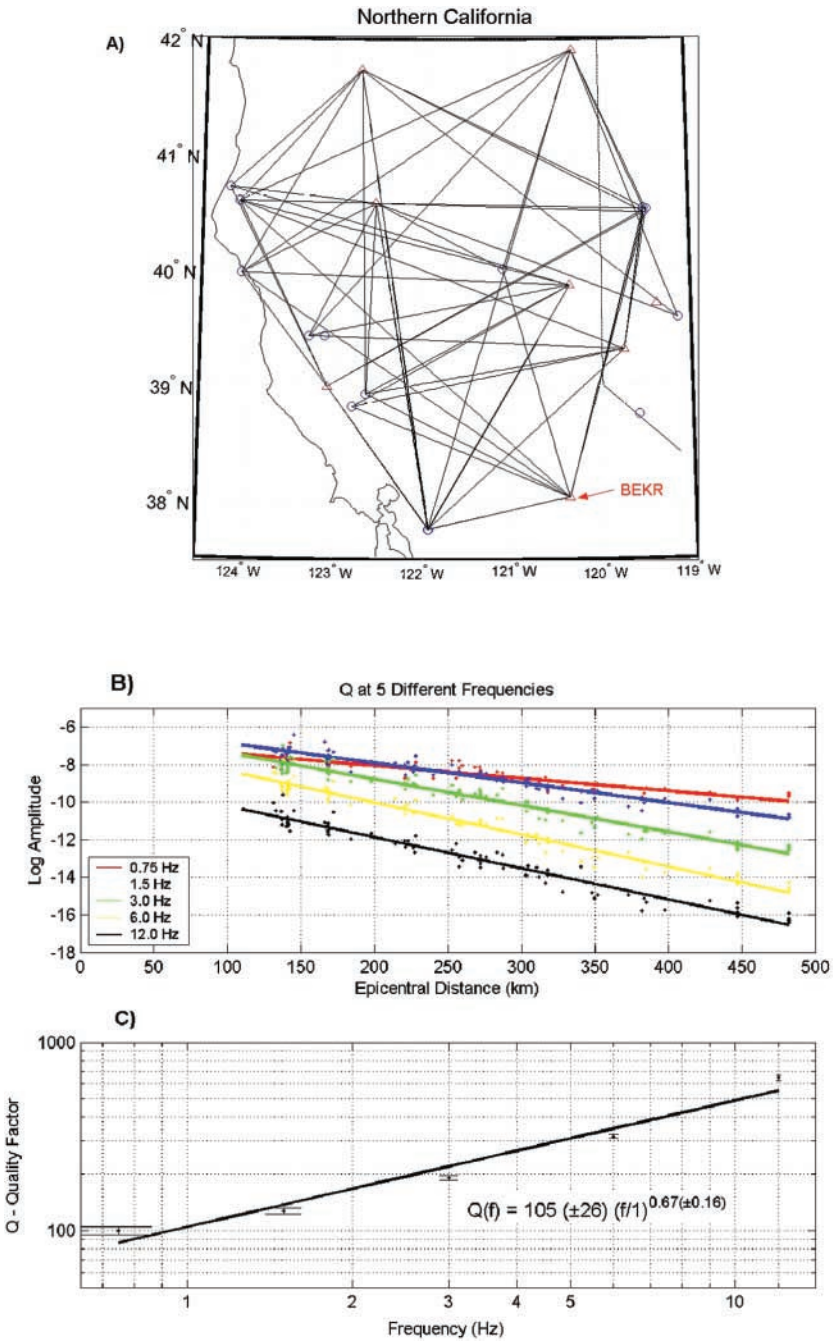

Figure 5. A, Northern California region ranges from 37°N to 42°N and from 119°W to 125°W. Triangles are broadband stations, circles are events, and lines represent *Lg* paths used in this study. There are 85 ray paths, 18 earthquakes, and seven stations in this 3 Hz sample region. B, Northern California *Lg* spectral amplitudes and corresponding best-fit lines that have been corrected for source and receiver terms. Best-fit line assumes a frequency-independent Q and $\gamma = 0.5$. C, The log–log graph f shows a frequency-dependent *Lg* Q for the northern California region with a best-fit function of $Q(f) = 105\ (\pm 26)\ (f/1)^{0.67(\pm 0.16)}$ between 0.75 and 12.0 Hz.

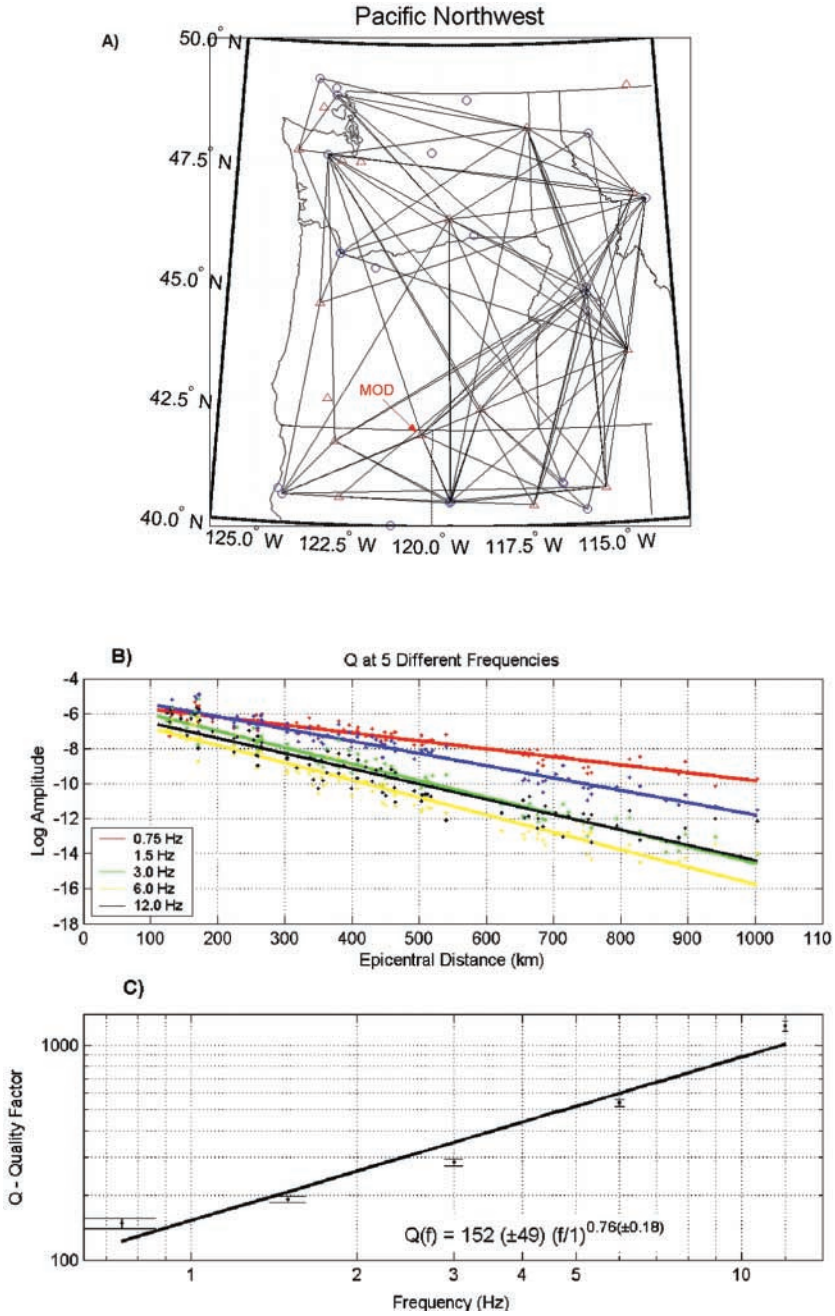

Figure 6. A, Pacific Northwest ray-path map at 3 Hz. This region ranges from 40°N to 50°N and 113°W to 126°W and contains 90 ray paths from 16 earthquakes recorded at 12 stations. Triangles, circles, and lines represent stations, earthquakes, and source–receiver ray paths, respectively. B, Results for Pacific Northwest showing *Lg* amplitudes for five different center frequencies and matching best-fit linear approximation assuming frequency-independent Q and $\gamma = 0.5$. Plot C shows the best-fit frequency-dependent *Lg* Q function of $Q(f) = 152\ (\pm 49)\ (f/1)^{0.76(\pm 0.18)}$.

are shown in Figure 5B. We selected station BEKR for the reference station, which is located on the border of California and Nevada. Results show that *Lg* Q increases from 100 (± 5) at 0.75 Hz to 650 (± 22) at 12.0 Hz. Northern California has a best-fit frequency-dependent *Lg* Q function of $Q(f) = 105\ (\pm 26)\ (f/1)^{0.67(\pm 0.16)}$ (Fig. 5C).

Pacific Northwest

The Pacific Northwest region is made up of Washington, Oregon, western Idaho, and northern California and Nevada and contains 16 earthquakes producing 90 ray paths at 12 stations (Fig. 6A). Figure 6B shows a best-fit linear approximation for the *Lg* spectral amplitude of five octaves corrected for receiver and source terms. The northeast corner of California contains the reference station MOD for this inversion. Values of Q increase from 148 (± 8) to 1233 (± 68) for the frequencies of 0.75 to 12.0 Hz.

The Pacific Northwest also has a low Q_0 value and a large frequency dependency with an equation of $Q(f) = 152\ (\pm 49)\ (f/1)^{0.76(\pm 0.18)}$ (Fig. 6C). The tectonic setting and the frequency-dependent function are both similar to those of the northern California region. Since there are no previous *Lg* Q studies in this area, a comparison to a similar tectonic region in south-central Alaska was required, which produced

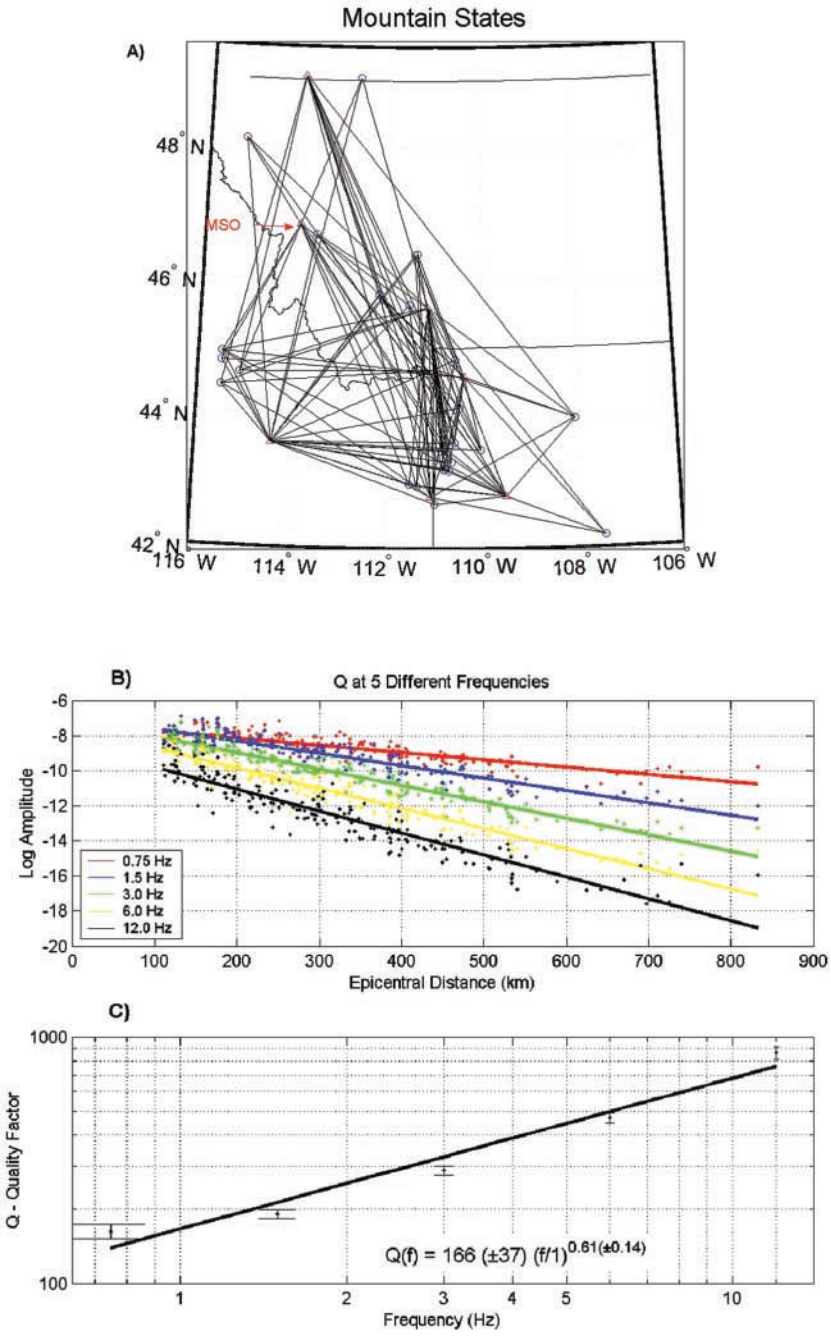

Figure 7. A, Ray-path map for the mountain states region with coordinates of 42°N to 50°N and 107°W to 116°W. This region is covered by 195 ray paths from 34 earthquakes recorded at 10 stations at 3 Hz. B, Mountain states region results for the center frequencies of 0.75, 1.5, 3.0, 6.0, and 12.0 Hz. The solid line represents the best-fit linear approximation assuming a frequency-independent Q and $\gamma = 0.5$. C shows the corresponding Q values plotted on a log–log scale with matching error bars and a best-fit frequency-dependent *Lg* Q function of $Q(f) = 166(\pm 37)\ (f/1)^{0.61(\pm 0.14)}$ between 0.75 and 12.0 Hz.

a frequency-dependent quality factor of $Q(f) = 220\ (\pm 30)\ f^{0.66(\pm 0.09)}$ (McNamara, 2000).

Mountain States

The mountain states region includes western Montana and Wyoming and eastern Idaho and is well covered with 195 ray paths caused by 34 earthquakes and recorded by 10 stations (Fig. 7A). This area is centered on the tectonically active Yellowstone hotspot in northwestern Wyoming and does not have a previously determined $Q(f)$ function.

The equation for the frequency-dependent Q for the mountain states is $Q(f) = 166\ (\pm 37)\ (f/1)^{0.61(\pm 0.14)}$ (Fig. 7C). Results show that *Lg* Q increases from 163 (± 11) at 0.75 Hz to 862 (± 50) at 12.0 Hz (Fig. 7B).

Central USA

Figure 8 shows a map and results for the central United States area, located in the Midwest of the continental United States, with coordinates 32°N to 40°N and 82°W to 103°W. This is a tectonically stable region with an active fault (New Madrid) that is well covered with 156 ray paths from 22 earthquakes recorded at 16 broadband stations. Q values for the New Madrid area are much higher than those of the western U.S. regions presented above, with Q values in-

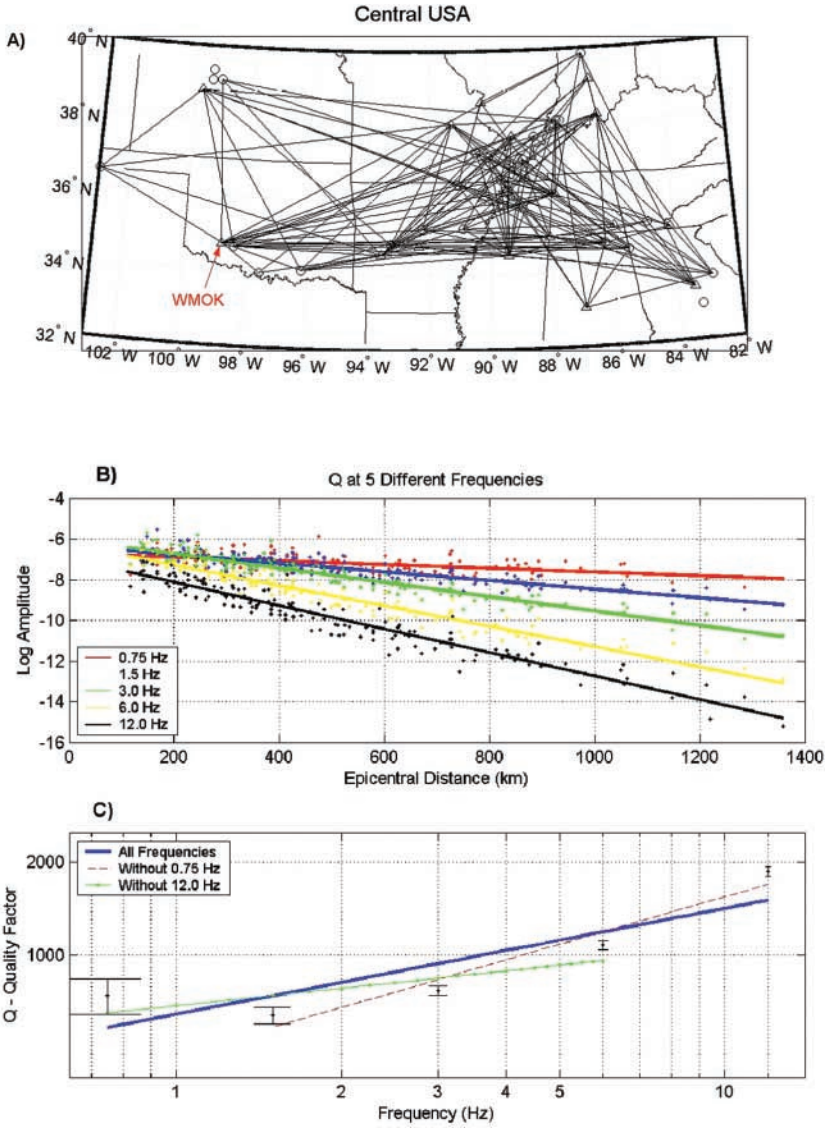

Figure 8. A, Path map for the central United States with 156 ray paths, 22 earthquakes, and 16 stations. This region is defined by the coordinates 32°N to 40°N and 82°W to 103°W. B, Central United States results showing *Lg* amplitudes corrected for receiver and source terms. The solid line is a L2 norm linear approximation assuming a frequency-independent Q and $\gamma = 0.5$. C is a log–log chart showing the values for Q at each frequency with matching errors and three best-fit lines. The Q terms on either end have a large error, so we fit three lines, one with all five frequencies included, one with the 0.75 Hz Q value removed, and one with the 12.0 Hz term removed. The frequency-dependent *Lg* Q function for this region using all five Q values is $Q(f) = 640\ (\pm 225)\ (f/1)^{0.344(\pm 0.22)}$ The frequency-dependent function with 0.75 Hz Q removed is $Q(f) = 470\ (\pm 127)\ (f/1)^{0.52(\pm 0.16)}$. And with the 12.0 Hz value removed, $Q(f) = 683\ (f/1)^{0.19}$.

creasing from 635 (±38) at 1.5 Hz to 1865 (±64) at 12.0 Hz. WMOK was used as the reference station and is located in southwestern Oklahoma. The equation for the best-fit linear approximation to the data is $Q(f) = 640\ (\pm 225)\ (f/1)^{0.344(\pm 0.22)}$, which reinforces our hypothesis of a high Q_0 value and a low η value for regions that are tectonically stable.

The Q value at 0.75 Hz appears to be an anomaly in this region, so we removed it and recalculated the *Lg* Q function (Fig. 8C). Between 1.0 and 12.0 Hz, the *Lg* Q function is $Q(f) = 470\ (\pm 127)\ (f/1)^{0.52(\pm 0.16)}$. The Q_0 error term decreased from 225 to 127, and the η error term decreased from 0.22 to 0.16. A non-frequency-dependent *Lg* Q was presented by Benz *et al.* (1997) with a mean Q value of 1291, while Singh and Herrmann (1983) found Q_0 to vary from 900 to 1350 at 1 Hz with a small frequency dependence described by $\eta = 0.1$ to 0.3. Our results are noticeably lower than those of other studies in the central United States, but we were able to find a frequency-dependent *Lg* Q.

Northeast USA

The northeast United States is a typical intraplate region with moderate seismicity (m_b usually less than 4.5), characterized by scattered epicenters (Shi *et al.*, 1996). This region can be seen in Figure 9A, represented by 12 earthquakes recorded at 12 stations for a total of 70 ray paths.

Results show *Lg* Q increasing from 676 (±170) at 0.75 Hz to 1843 (±130) at 12.0 Hz (Fig. 9c). Large jackknife standard deviations reinforce our hypothesis that station instrumentation might vary over time without our knowledge. Station NCB was chosen for the reference station and is located in upstate New York. The linear equation that best represents our data on a log–log plot is $Q(f) = 650\ (\pm 143)\ (f/1)^{0.36(\pm 0.14)}$ (Fig. 9C). Shi *et al.* (1996) found an average frequency-dependent Q_0 of 723 and an average η of 0.42 for a region similar to the one used in this study.

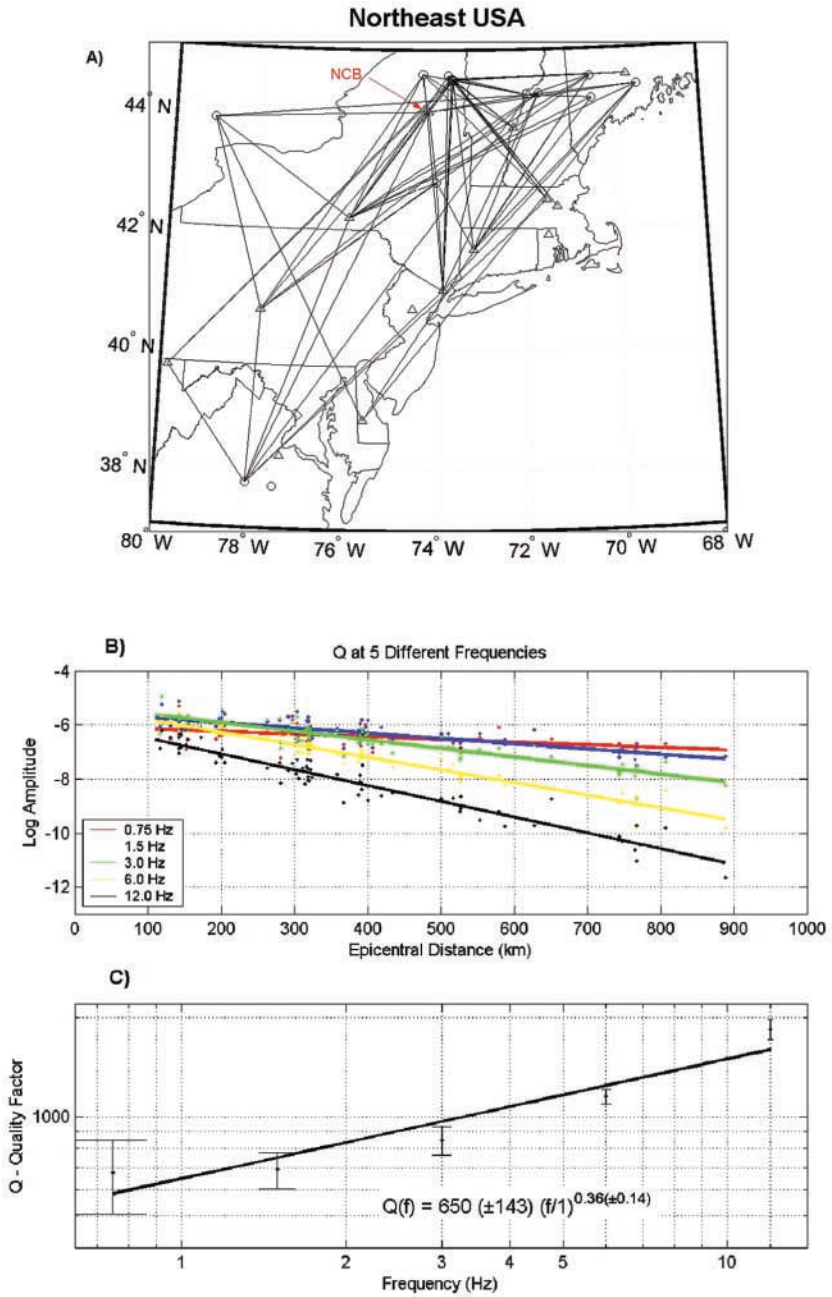

Figure 9. A, Northeast U.S. region ray-path coverage map at 3 Hz. Solid lines indicate source–receiver raypaths, circles represent earthquakes, and triangles symbolize stations. This region is limited to the coordinates of 37°N to 45°N and 68°W to 80°W and is defined by 70 ray paths from 12 earthquakes recorded at 12 stations. B, Northeast U.S. *Lg* spectral amplitudes (dots) at 0.75, 1.5, 3.0, 6.0, and 12.0 Hz, corrected for source and receiver terms. Solid line is best-fit linear trend for data assuming frequency-independent Q and $\gamma = 0.5$. C contains the five values for Q at each center frequency with corresponding error bars and a best-fit linear trend plotted on a log–log graph to show a frequency-dependent Q. The best-fit frequency-dependent *Lg* Q function is $Q(f) = 650\ (\pm 143)\ (f/1)^{0.36(\pm 0.14)}$ between 0.75 and 12.0 Hz.

Discussion

Southern and northern California, the Pacific Northwest, the mountain states, and the Basin and Range Province are all well described by low *Lg* Q and strong frequency dependence, while the central and northeast United States are best described by high *Lg* Q and weak frequency dependence (Fig. 10). Furthermore, *Lg* Q exhibits a minimum between 0.75 Hz and 1.5 Hz and increases in value up to 12.0 Hz for all seven regions studied in this article. A comparison of *Lg* amplitude decay in the seven different regions reinforces our findings, since amplitudes decay much faster in the western United States than in the eastern United States (Fig. 11).

Although the linear fits to the *Lg* amplitudes are good, the central and northeast U.S. regions have the largest standard deviations of the seven regions. Raypath coverage is not an issue for the central United States, since this region has over 150 ray paths. Various smaller regions centered around the New Madrid fault were inverted for *Lg* Q to test for stability, but we found higher standard deviations with similar *Lg* Q values. High-frequency surface-wave contamination might be responsible for the relatively high variation in standard deviation for this region.

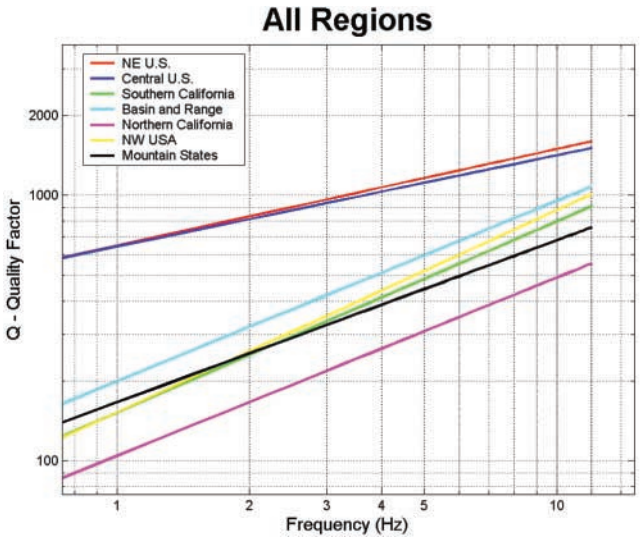

Figure 10. Log–log graph showing all regions described. Notice steeper slope and lower Q values for the active tectonic regions in the western United States versus the flatter slopes and higher Q values of central and northeastern United States.

The northeast United States region has less than half the ray paths of the central United States, with only 70 ray paths covering this region. Not all stations in this area are maintained by the U.S. Geological Survey, therefore we lack sufficient information to properly identify the response on these broadband stations. Consequently, high standard deviations might be caused by any one or a combination of surface-wave contamination, ray-path coverage, or unknown instrument response. Shi *et al.* (1996) divided this region into three subregions consisting of the Adirondack Mountains (Q = 905 $f^{0.40}$), the central Appalachian Province (Q = 561–586 $f^{0.46–0.47}$), and the northern New England Appalachians (Q = 705 $f^{0.41}$). Our frequency-dependent function falls roughly in the middle of their results with a value of $Q(f)$ = 650 ($\pm$143) $(f/1)^{0.36(\pm 0.14)}$. The variation in results is probably due to different ray paths and coverage density.

The Pacific Northwest and the northern California regions have not been extensively studied in the past for *Lg* Q, but results similar to those of other comparable tectonic regions, such as south-central Alaska, support our results. The mountain states region is influenced by the high attenuation of the Yellowstone hotspot and has not been recently studied with this kind of ray-path coverage. The remaining two regions (southern California and the Basin and Range Province) all exhibit frequency-dependent *Lg* functions that are similar to those of previous studies.

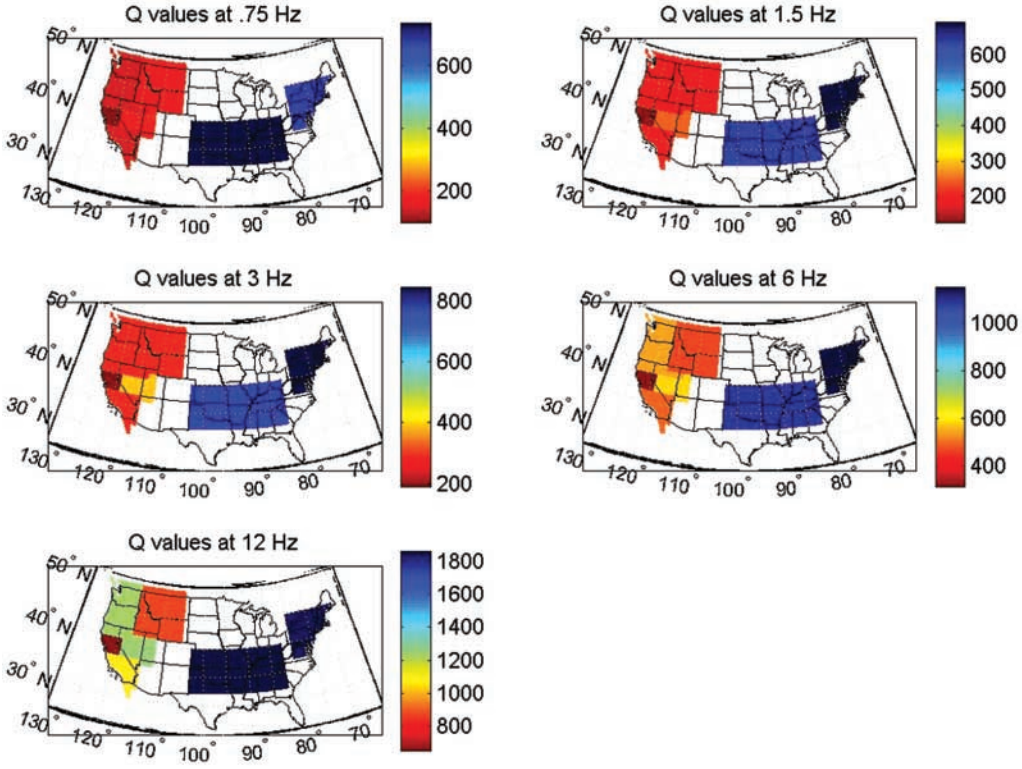

Figure 11. Q values for the seven different regions presented, shown on a map of the continental United States for each of the five center frequencies (0.75, 1.5, 3.0, 6.0, and 12.0 Hz). Red denotes low Q values and blue represents high Q values.

Conclusion

Our objective in this article was to document differences in *Lg* attenuation between seven different tectonic regions in the continental United States. Standardized instrumentation and consistent processing provide attenuation functions that can be used in a variety of applications including local magnitude estimates, earthquake hazard assessment in populated areas, and structural engineering applications. Further work will include obtaining more data to determine *Lg Q* for the remaining tectonic areas of the United States, and to expand the technique to a 2D tomographic inversion of the entire continental United States.

Acknowledgments

We thank the U.S. Geological Survey for supporting summer internships and providing data used for this research.

References

Aki, K. (1980). Scattering and attenuation of shear waves in the lithosphere, *J. Geophys. Res.* **85,** 6496–6504.

Atkinson, G., and R. Mereu (1992). The shape of ground motion attenuation curves in southeastern Canada, *Bull. Seism. Soc. Am.* **82,** 2014–2031.

Benz, H., A. Frankel, and D. Boore (1997). Regional *Lg* attenuation of the continental United States, *Bull. Seism. Soc. Am* **87,** 606–619.

Chavez, D., and K. Priestley (1986). Measurement of frequency dependent *Lg* attenuation in the Great Basin, *Geophys. Res. Lett.* **13,** 551–554.

Christensen, N., and W. Mooney (1995). Seismic velocity structure and composition of the continental crust: a global view, *J. Geophys. Res.* **100,** 9761–9788.

Efron, B., and R. J. Tibshirani (1993). *An Introduction to the Bootstrap*, CRC, Boca Raton, Florida.

Ferdinand, R. W. (1998). Average attenuation of 0.7–5.0 Hz *Lg* waves and magnitude scale determination for the region bounding the western branch of the East African Rift, *Geophys. J. Int.* **134,** 818–830.

Frankel, A. (1991). Mechanisms of seismic attenuation in the crust: scattering and anelasticity in New York state, South Africa, and Southern California, *J. Geophys. Res.* **96,** 6269–6289.

Frankel, A., A. McGarr, J. Bicknell, J. Mori, L. Seeber, and E. Cranswick (1990). Attenuation of high-frequency shear waves in the crust: measurements from New York state, South Africa, and southern California, *J. Geophys. Res.* **95,** 17441–17457.

Gregersen, S. (1984). *Lg*-wave propagation and crustal structure differences near Denmark and the North Sea, *Geophys. J. R. Astr. Soc.* **79,** 217–234.

Gutenberg, B. (1955). Channel waves in the Earth's crust, *Geophysics* **20,** 283–294.

Kennett, B. (1986). *Lg* waves and structural boundaries, *Bull Seism. Soc. Am.* **76,** 1133–1141.

McNamara, D., and W. Walter (2001). Mapping crustal heterogeneity using *Lg* propagation efficiency throughout the Middle East, Mediterranean, Southern Europe and Northern Africa, Pageoph **158,** 1165–1188.

McNamara, D. E. (2000). Frequency dependent *Lg* attenuation in south-central Alaska, *Geophys. Res. Lett.* **27,** 3949–3952.

McNamara, D. E., and W. R. Walter (2001). Mapping crustal heterogeneity using *Lg* propagation efficiency throughout the middle east, Mediterranean, southern Eruope, and northern Africa, *PAGEOPH* **158,** 1165–1188.

McNamara, D. E., T. J. Owens, and W. R. Walter (1996). Propagation characteristics of *Lg* across the Tibetan Plateau, *Bull. Seism. Soc. Am* **86,** 457–469.

Mitchell, B. (1975). Regional Rayleigh wave attenuation in North America, *J. Geophys. Res.* **80,** 4904–4916.

Nuttli, O. (1973). Seismic wave attenuation and magnitude relations for eastern North America, *J. Geophys. Res.* **78,** 876–885.

Nuttli, O., G. Bollinger, and D. Griffiths (1979). On the relation between modified mercalli intensity and body wave magnitude, *Bull. Seism. Soc. Am.* **69,** 893–910.

Oliver, J., and M. Ewing (1957). Higher modes of continental Rayleigh waves, *Bull. Seism. Soc. Am* **47,** 187–204.

Press, F., and M. Ewing (1952). Two slow surface waves across North America, *Bull. Seism. Soc. Am* **42,** 219–228.

Reese, C. C., R. R. Rapine, and J. F. Ni (1999). Lateral variation of *Pn* and *Lg* attenuation at the CDSN Station LSA, *Bull. Seism. Soc. Am.* **89,** 325–330.

Shi, J., W. Kim, and P. Richards (1996). Variability of crustal attenuation in the northeastern United States from *Lg* waves, *J. Geophys. Res.* **101,** 25,231–25,242.

Singh, S., and R. Herrmann (1983). Regionalization of crustal coda *Q* in the continental United States, *J. Geophys. Res.* **88,** 527–538.

Smithson, S. (1978). Modeling continental crust: structural and chemical constraints, *Geophys. Res. Lett.* **9,** 749–752.

Xie, J. K., and B. J. Mitchell (1990). Attenuation of multiphase surface waves in the Basin and Range province, part I: *Lg* and *Lg* coda, *Geophys. J. Int.* **102,** 121–137.

University of Wyoming
Laramie, Wyoming 82071
drericks@uwyo.edu
(D.E.)

U.S. Geological Survey
Golden, Colorado 80225
(D.E.M., H.M.B.)

Manuscript received 14 October 2003.